Binding Constants from Zone Transport of Interacting Molecules†

J. Eisinger* and W. E. Blumberg

ABSTRACT: A semiempirical theory based on computer simulations is presented and experimentally confirmed, which permits the evaluation of binding constants (K) from experimental parameters obtained from gel electrophoresis (or other linear differential transport) of interacting molecules. Experimental protocols for determination of K for reactions of the type A + B $\rightleftarrows$ C under rapid equilibrium conditions are offered for homodromous and heterodromous reactants. These protocols make use of observable parameters such as positions of and molarities at zone maxima, and fractions of molecules which have traveled more than a certain distance. These methods of analysis are suitable for optical, radioactive, or other detection techniques.

The past 2 decades have seen a great increase in the use of techniques which make use of differential mass transport to separate biological molecules for analytical as well as preparative purposes. These methods include gel filtration, centrifugation, moving boundary and zonal electrophoresis, and chromatography in paper and starch media and, more particularly, gel electrophoresis. In all of these techniques the transport properties are, in principle, sensitive to interactions between the transported molecules with each other and with solvent molecules. Such interactions can lead to important artifacts such as altered transport velocities, extra zones, and distortion of zones and boundaries, which have received careful attention. On the other hand, there have been relatively few determinations of equilibrium constants which made use of these phenomena. The reasons for this are, on the one hand, the fact that the available experimental techniques were often slow, expensive, and not sufficiently precise, and, on the other hand, that the differential equations which represent the transport of interacting and diffusing zones are not integrable in a closed form. As a result, explicit expressions which give association constants as a function of experimental parameters do not exist.

Recent advances in the technology of gel electrophoresis have overcome the experimental problems. Gels can be formed quite reproducibly, quickly, and cheaply. They can be scanned for absorption, fluorescence, or radioactivity with ease, and, for many biologically important molecules, with considerable resolution.

We have investigated zone transport with a view of using it as a simple, practical method for determining equilibrium constants under a wide variety of conditions. To this end we have derived approximate analytical relationships between certain experimental parameters and the association constant (K). These results served as a guide in analyzing zones of interacting molecules simulated by a computer program under more realistic conditions, including diffusion. In this way we developed several experimental protocols which permit the semiempirical determination of K from some readily observable experimental parameters.

The sensitivity of differential mass transport experiments to interactions between various species was first noted by Tiselius (1930) and by Longsworth and McInnes (1942). Detailed investigations into the shapes of zones and boundaries of interacting molecules were made by Gilbert and Jenkins (1959) using an analytical approach. After computers became generally available, Kegeles, Bethune, Cann, Goad, and others used them to calculate zone and boundary shapes under a variety of conditions (Bethune and Kegeles, 1961a–c; Cann and Goad, 1965; Oberhauser *et al.*, 1965; Kegeles *et al.*, 1967). This work has been reviewed by Nichol *et al.* (1964), and some of the characteristics of zone transport of interacting species discussed in the present paper are analogous to features in the sedimentation and countercurrent distribution patterns summarized there.

The present paper concentrates on a particularly simple case of molecular interaction which is of wide applicability, namely on interactions of the type A + B $\rightleftarrows$ C under conditions of rapid equilibrium (see below). We have usually assumed that the transport velocities of the reactants are greater than or equal to that of the complex although it is possible to extend the present theory to cases where this is not the case.

The range of experimental situations to which the present methods of determining K is applicable is very wide so that it is impossible to make a general comparison to other methods. In as much as the most promising applications lie in gel electrophoresis experiments (see section 4), it is worthwhile to compare this method with equilibrium dialysis which has been used for some of the same binding experiments (*cf.* binding of complementary oligonucleotides to RNA). The basic requirement of equilibrium dialysis is that the membrane permeability be very different for A (or B) and C and that the permeability to one of the reactants is sufficiently great to permit equilibrium to be reached in a reasonable time. The corresponding requirement for gel electrophoresis is that there be a measurable difference in the electrophoretic mobilities of two of the species A, B, and C. In determining the association between oligonucleotides and RNA, both methods are reasonably cheap and require comparably small quantities of the synthetic oligomers although gel electrophoresis has greater possibilities of further miniaturization (*e.g.*, by the use of gel fibers). Dialysis is slower and becomes prohibitively slow for pentamers and longer oligomers. It is moreover limited to work at high ionic strength while gel electrophoresis can be used over a wide range of ionic strength, as long as the two interacting molecules have appreciably

† From Bell Laboratories, Murray Hill, New Jersey 07974. *Received March 22, 1973.*

different electrophoretic mobilities. Gel electrophoresis offers the additional advantage that it reveals aggregation effects which might go unnoticed in dialysis experiments.

In sections 1 and 3 we shall present concentration profiles of interacting zones in one-dimensional zone transport experiments for the various sets of loading ratios and velocity relationships among the reactants which one may encounter. These profiles are obtained by simulating the transport experiment by means of a computer as outlined in the remainder of this section. By using certain parametrizations of the computer simulated results, which are in many cases suggested by algebraic solutions for simplified models (*cf.* Appendices 2 and 3), it is possible to obtain graphs from which association constants may be obtained from readily observable experimental parameters, such as peak concentrations within the gel or separations between zone maxima measured along the gel. These experimental parameters are determined by scanning the concentration profile of one or both reactants along the length of the gel using a predetermined physical property such as optical density, fluorescence, radioactivity, etc. In the final section we offer some experimental results which illustrate the applicability of the method to various biochemical problems and provide examples of experimental methods for scanning gels.

Principles. In the present paper we shall focus our attention on reactions of the type

$$A + B \underset{k_r}{\overset{k_f}{\rightleftharpoons}} C \tag{1}$$

where k_f and k_r refer to the forward (bimolecular) and reverse rates. This type of reaction has been classified according to the relative and absolute magnitudes of k_f and k_r by Nichol *et al.* (1964), but we will confine ourselves to the frequently encountered case in which k_f and k_r are both large compared with typical transport rates. In gel electrophoresis this rate is $\mu E/w$ or about 10^{-2} sec^{-1} where μ is the gel electrophoretic mobility, E the electric field, and w the width of a zone. In other words, we shall assume rapid equilibrium conditions for eq 1.

In order to determine the association constant $K = k_f/k_r$ (M^{-1}), it is necessary to select a chromatographic system in which the electrophoretic mobility of one of the species participating in reaction 1 differs appreciably from those of the other two. In gel electrophoresis, for instance, the ionic strength and pH of the buffer as well as the consistency of the gel will determine the relative and absolute velocities of the loaded molecules and their complex (Chrambach and Rodbard, 1971; Richards and Lecanidou, 1971). The various experimental situations which arise are conveniently divided into those involving homodromous and heterodromous reactants.[1] In dimerization and pseudodimerization reactions, $v_A = v_B > v_C$ while in ligand binding the macromolecules, for instance, one encounters velocity relationships of the type $v_A > v_B = v_C$ or $v_A > v_B \gtrless v_C$ with the former a common limiting case of the latter.[2] These cases will be examined individually in the sections to follow. The computer-simulated experiments, properly parametrized, are summarized in graphical solutions, which are in turn fitted by semiempirical relationships which show the dependence of the equilibrium constant on various experimental parameters. These relationships for the various cases will be summarized at the end of the paper.

Theoretical Formulation. We derive the basic equations which permit the computer simulation of zone transport of interacting molecules with the assumption that at time $t = 0$ the A and B molecules occupy zones which may overlap. The shape of each zone is assumed to be gaussian with a width w_0 at half-maximum. In other words, the concentration distributions in the starting zones are

$$c_{A,B}(t = 0) = c_{max} \exp(-\delta^2 x^2) \tag{2}$$

where $\delta = 2\sqrt{\ln 2}/w_0$. In gel electrophoresis, A and B are generally loaded by layering them on the gel, and if A and B enter the gel at different rates a starting zone like that given by eq 2 may be impossible to achieve in practice. This is particularly important if A and B are small and large ions, respectively. It will be seen below that this difficulty may be overcome by giving B a headstart which is sufficient to establish a zone within the gel before the faster A ions are loaded.

In the presence of a constant force field the concentrations of A, B, and C at a particular distance x from the starting position will have a time dependence which reflects the concentration gain (or loss) due to their mobility, diffusion, and the forward and reverse rates of the reaction given in eq 1.

$$\frac{\partial c_A}{\partial t} = v_A\frac{\partial c_A}{\partial x} + D_A\frac{\partial^2 c_A}{\partial x^2} - k_f c_A c_B + k_r c_C \tag{3a}$$

$$\frac{\partial c_B}{\partial t} = v_B\frac{\partial c_B}{\partial x} + D_B\frac{\partial^2 c_B}{\partial x^2} - k_f c_A c_B + k_r c_C \tag{3b}$$

$$\frac{\partial c_C}{\partial t} = v_C\frac{\partial c_C}{\partial x} + D_C\frac{\partial^2 c_C}{\partial x^2} + k_f c_A c_B - k_r c_C \tag{3c}$$

Here v_A, v_B, and v_C are the velocities of A, B, and C in the presence of the force field, and D_A, D_B, and D_C are the diffusion coefficients of A, B, and C. In gel electrophoresis $v_A = \mu_A E$, etc. In rapid equilibrium conditions the concentrations of the reactants and their complex at any particular time and gel position are related by the expressions

$$c_A c_B/c_C = k_r/k_f = 1/K \tag{4}$$

These simultaneous differential equations were approximated by finite difference equations as outlined in Appendix 1 and digital and graphical solutions were obtained at a time sharing terminal of a Honeywell 6000 computer with a graphic interface.

While this approach can produce solutions for any set of starting conditions and parameters, many practical situations can be approximated by considering the simple limiting cases which will be examined in some detail below.

Stoichiometry of Reactants. The present paper offers protocols for determining the association constant of reactions of the type given in eq 1. Before applying these it is of course necessary to ensure that one is not dealing with reactions of the type

$$A + nB \rightleftharpoons C \tag{1a}$$

or

$$nA + B \rightleftharpoons C \tag{1b}$$

($n > 1$)

As in other techniques for studying binding, reactions corresponding to eq 1a,b are distinguishable from those corre-

[1] Homodromous and heterodromous ($\delta\rho\acute{o}\mu\omega$s, a running) refer to the relative speeds of the reactant molecules in the chosen chromatographic system.

[2] We shall use the convention that A is the fastest reactant and C is the complex which may be faster or slower than the reactants. It may even move in the opposite direction ($v_C < 0$).

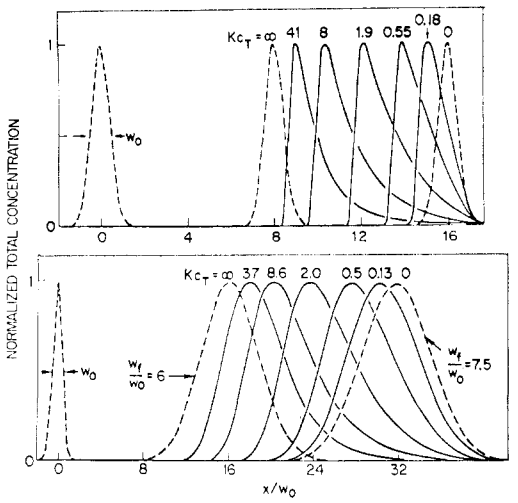

FIGURE 1: Families of normalized total concentration profiles ($c_T = c_A + c_B + c_C$) following zone transport (*e.g.*, gel electrophoresis) for periods during which the monomers (A or B) traveled distances $16w_0$ (upper half) and $32w_0$ (lower half), respectively. Homodromous reactants A and B were loaded in stoichiometrically equal amounts, and the complex C has a velocity which is half the velocity of A or B. Diffusion is neglected in the upper set of profiles and accounts for an eightfold increase in the monomer zone width for the lower set, the diffusion broadening of the complex being assumed to be two-thirds as great. Each concentration profile corresponds to a particular value of Kc_T. The typical zone profile is skewed by monomers escaping the complex zone in a forward direction. The trailing edge is sharpened as the molecules, upon dissociation, speed up and rejoin the complex zone. The symmetrical dashed zones corresponding to Kc_T values 0 and ∞ are peaked at $x = x_A$ and x_C, respectively. It is clear that the velocity of the complex zone is a sensitive function of the association constant. Note that while this figure as well as Figures 3 and 5 are based on computer simulations in which $v_C = v_A/2 = v_B/2$, the fractional retardations obtained here are independent of the value of v_C as long as $v_C < v_A$ and the experiment is carried on long enough to separate x_A and x_C sufficiently. Note also that the fractional retardation ($\Delta x/\Delta x_{AC}$) for a particular value of Kc_T is virtually independent of diffusion.

sponding to eq 1 only if experiments are performed in the domain in which nKc is of the order of unity. (Here c is the concentration of the reactant which is suspected of harboring multiple binding sites, *e.g.*, c_B in eq 1a.) This follows from the fact that the fraction of A molecules bound (f) is virtually independent of c_A if $(c_A/c_B) \ll 1$. In this so-called low concentration limit, measurement of f (or any equivalent parameter) can only yield nK, where it is assumed that the n binding sites of B are independent and have the same K.

Appendix 4 offers protocols which permit the experimenter to check if values of K obtained by analysis of gel electrophoresis experiments are consistent with eq 1. While it is advisable to ensure the applicability of the experimental protocols offered here in this way, the stoichiometry of the reactants is in many cases known from other considerations.

1. Binding of Homodromous Reactants (Pseudodimerization)

1a. The Diffusionless, Stoichiometrically Equal Case. This limiting case is characterized by A and B having very similar velocities, with C traveling somewhat more slowly, and the amounts of A and B loaded (l_A and l_B) being approximately equal. That is,

$$v_A \approx v_B > v_C$$

$$l_A/l_B \approx 1$$

in the gel electrophoresis of molecules such as proteins or tRNA, dimers have an electrophoretic mobility which is about 0.6 of that of the monomers in 10% polyacrylamide gels. Since A and B can be expected to enter the gel at the same rate, the starting condition given by eq 2 is approximated quite closely in the first few millimeters of the gel some time after loading and the application of the electric field. In 10% polyacrylamide gels this time is found to be approximately 20 min at 5 V/cm for tRNA molecules. The starting width of the concentration profile may be determined experimentally at this time by scanning the gel in its quartz tube with ultraviolet light, as may the concentration profiles at any other time. This nondestructive optical scanning is of course only capable of giving the x dependence of $\epsilon_A c_A + \epsilon_B c_B + \epsilon_C c_C$, where ϵ_A, ϵ_B, and ϵ_C are the molar extinction coefficients of A, B, and C at some wavelength. In the dimerization case it is usually assumed that $\epsilon_C \approx \epsilon_A + \epsilon_B$ so that an optical scan gives a profile proportional to $c_T = c_A + c_B$, where the subscript T refers to total (*i.e.*, bound *and* free) concentrations.

Figure 1 presents graphical solutions for the pseudodimerization case where the reactants are loaded in stoichiometrically equal amounts and there is no diffusion. It is seen that the relevant parameter is the dimensionless product $Kc_{T_{max}} = K(c_{A_{max}} + c_{B_{max}})$ and that the effective electrophoretic mobility of the compound zone is intermediate between that of A and C. $c_{A_{max}}$ is the concentration of A at the peak of the zone.[3] When Kc_T is very small, the velocity of the compound zone approaches v_A and when it is very large it approaches v_C. It is seen that the greatest precision for the determination of K is achieved when Kc_T is between 1 and 10. In practice one may load a series of identical gels with different concentrations of equimolar mixtures of A and B. This permits one to estimate v_C by extrapolation to infinite concentrations.

The profiles shown in Figure 1 and in similar succeeding ones were obtained with $v_A = v_B = 2v_C$, where the magnitude of v_C was chosen to produce a pleasing figure. It should be pointed out, however, that if the retardation $\Delta x = x_A - x_{max}$ is expressed as a fraction of $\Delta x_{AC} = x_A - x_C$ the results are independent of the magnitude of v_C even if v_C is larger than v_A.

The asymmetric shapes of the compound zones shown in Figure 1 may be understood qualitatively as arising from dissociation of the complex C at the zone edges which leads to a sharp trailing edge and a diffuse forward edge (DeVault, 1943). It was suggested earlier (Eisinger, 1971) that the velocity of the compound zone would be given simply by the relationship

$$v = fv_C + (1 - f)v_A \tag{5}$$

where f is the fraction of the time during which A and B are complexed to form C. This fraction will therefore be equal to the fraction of A (or B) molecules bound in the complex at any particular time. From this it follows that at any time during a zone transport experiment (*e.g.*, gel electrophoresis)

$$f = \frac{v_A - v}{v_A - v_C} = \frac{x_A - x}{x_A - x_C} = \frac{\Delta x}{\Delta x_{AC}} \tag{6}$$

where x is the position of the peak of the compound zone. This expression is shown as a straight dashed line in Figure 2.

[3] In the remainder of the paper the subscript max will often be omitted and it will be understood that the parameter c_B, particularly in the expressions involving Kc_B, refers to the peak concentration of B in the zone.

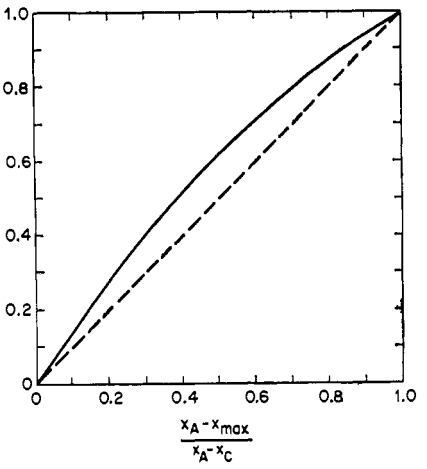

FIGURE 2: Comparison between the fractional retardation, $\Delta x/\Delta x_{AC}$, of the peaks of the complex zones shown in Figure 1 with the fraction of A molecules bound (—). If one uses the median positions of the complex zones in determining the retardation, the points fall on the dashed straight line which is the linear relationship postulated in eq 5.

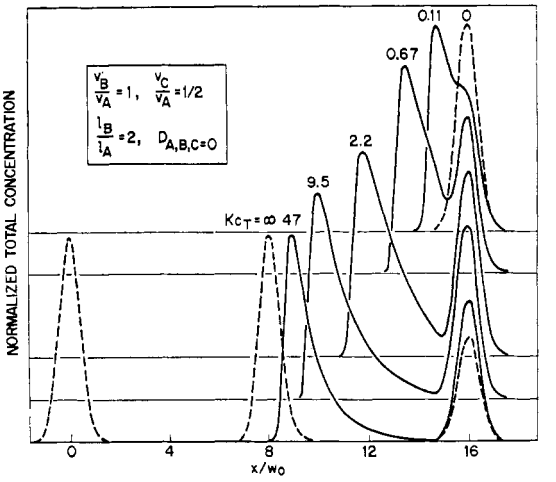

FIGURE 3: Normalized total concentration profiles for homodromous reactants in the absence of diffusion with one of the reactants loaded in a twofold molar excess. The excess monomer travels ahead of the complex zone but the peaks of the complex zones are not greatly perturbed from the positions shown in Figure 1. Thus the determination of K is not greatly influenced by stoichiometric inequality.

The same figure shows values of the coordinates obtained from the peaks of the computer-generated profiles like the ones shown in Figure 1. It is clear that the simple argument on which eq 5 is based comes close to the truth. In fact, an almost perfect fit with eq 6 and the dashed line in Figure 2 is obtained if x_{max} is interpreted to be the position of the centroid of the complex zone, rather than the position of its peak.

In this stoichiometric limit an expression for f may be obtained from the binding equation

$$f = 1 - \frac{\sqrt{1 + 4Kc_A} - 1}{2Kc_A} \tag{7}$$

where $c_A = c_B$. Substituting eq 7 in eq 5 one obtains the following approximate expressions for the retardation ($c_T = c_A + c_B = 2c_A$).

$$\Delta x = \left\{1 - \frac{\sqrt{1 + 2Kc_T} - 1}{Kc_T}\right\}\Delta x_{AC} \tag{8}$$

or

$$Kc_T = \frac{1 + \sqrt{(1 - \Delta x/\Delta x_{AC})^2 + 1}}{(1 - \Delta x/\Delta x_{AC})^2} \tag{9}$$

It is of considerable heuristic value to note that the eq 6, 8, and 9 which are based on simple considerations of the equilibrium of interacting molecules within a zone come close to mirroring simulated and actual gel electrophoresis experiments. In practice it is, however, more accurate and more convenient to use the methods suggested in section 1c to relate Kc_T to $\Delta x/\Delta x_{AC}$.

1b. Effects of Diffusion and Failure to Achieve Stoichiometric Equality. The simulation patterns broaden when diffusion effects are included but they retain their most characteristic features.[4] The conclusion that a compound zone with a peak halfway between that of A (or B) and C appears when Kc_T is approximately 2 is almost independent of the magnitude of the diffusion coefficients. This is illustrated in Figure 1.

Figure 3 shows that the violation of the stoichiometric requirement for dimerization leads to the appearance of an additional zone corresponding to the excess reactant which escaped during the early stages of the electrophoresis. In practice, if the excess of one of the reactants over the other does not exceed a factor of 2, equilibrium constants may still be determined from the total optical profiles by the methods outlined above by simply disregarding the extra peak.

1c. Graphical Solutions for Homodromous Reactants and Equimolar Loading. If one measures the positions of the peaks of the complex zones, following electrophoresis (x_{max}) as well as the positions of the monomer peak under identical conditions and the (extrapolated) value of x_C, the position corresponding to the complex zone in the high concentration limit, one may plot the quantity $(x_A - x_{max})/(x_A - x_C)$ *vs.* Kc_T. This is done in Figure 4. The solid curve for which diffusion effects are neglected is found to be independent of the relative values of x_A ($= x_B$) and x_C and the zone widths. The position of the complex zone is seen to be midway between those of the monomer and the binary complex when $Kc_T \approx 2$. This curve is useful for determining Kc_T, and hence K, for the range $0.5 \lesssim Kc_T \lesssim 20$. It may alternatively be represented by the following expressions to an accuracy of a few per cent

$$Kc_T = 2.2[\Delta x_{AC}/\Delta x - 1]^{-1.35} \tag{10}$$

or

$$\Delta x = \Delta x_{AC}/[1 + 1.8(Kc_T)^{-0.74}] \tag{11}$$

where we have written $\Delta x = x_A - x_{max}$.

Of the two remaining curves shown in Figure 4, one corresponds to the inclusion of considerable diffusion leading to a zone broadening of a factor of 8 during the course of the electrophoresis and the other corresponds to nonstoichiometric loading of the gel, with the load of B exceeding that of A by a factor of 2. It is remarkable that the results obtained for these conditions have a barely noticeable effect on the

[4] Most simulated concentration profiles are shown at times for which the fastest reactant has traveled a distance of $x = 16w_0$ from the starting position given by eq 1. Diffusion broadening is assumed to be proportional to the square root of the running time and its magnitude is measured by w_f/w_0, where w_f is the final width of the zone of a particular reactant or complex at the running time for which a simulation is shown.

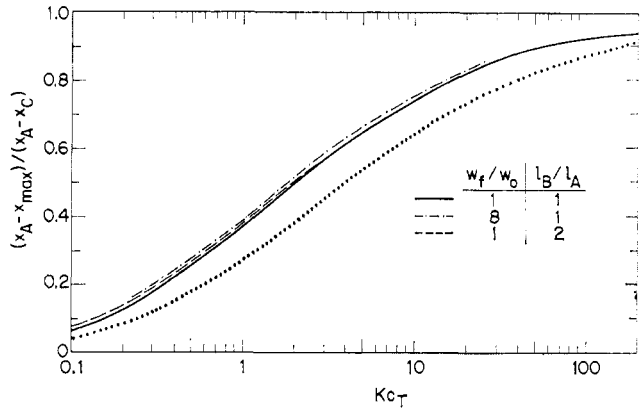

FIGURE 4: Fractional retardation of the compound zone containing equimolar concentration of homodromous reactants. The solid curve gives the retardation of the zone peaks in the absence of diffusion. In the presence of diffusion (*cf.* Figure 1) which leads to a 7.5-fold increase of the monomeric zone widths this curve changes only minimally and the corresponding retardations are shown thus -·-·-. If the load exceeds that of A by a factor of 2 (*cf.* Figure 3) the results fall on the dashed curve (– – –). The dotted curve shows the fractional retardation calculated from the approximate formula $f = \Delta x/\Delta x_{AC}$ (eq 8 in the text). If the median positions rather than the maxima of the compound zones are used in determining the fractional retardation the asymmetrical compound zones, the results would almost coincide with this curve (*cf.* Figure 2). The solid curve in this figure is seen to be adequate for determining K from experimental values for $\Delta x/\Delta x_{AC}$ as long as A and B are approximately homodromous and are loaded in approximately stoichiometric amounts.

solid curve shown in the figure which corresponds to the diffusionless case with stoichiometric equality. If A and B are only approximately homodromous ($|v_A - v_B| \lesssim 0.1(v_A - v_C)$) the foregoing results continue to hold with x_A set equal to $(x_A + x_B)/2$.

1d. Homodromous Reactants in the Low Concentration Limit. In certain binding experiments it may be possible to monitor c_A *or* c_B rather than their sum (for instance, if one of the reactants is radioactive or if one of the reactants has a unique optical property). We refer to this unique property of A or B as its "label." If A and B are present in approximately equal amounts, the compound zone may be identified as before, and a value for $Kc_A = Kc_T/2$ (and hence K) is found as before from the curves shown in Figure 4. Another common situation is the low concentration limit for homodromous reactants in which the amount of A loaded on the gel, l_A, is

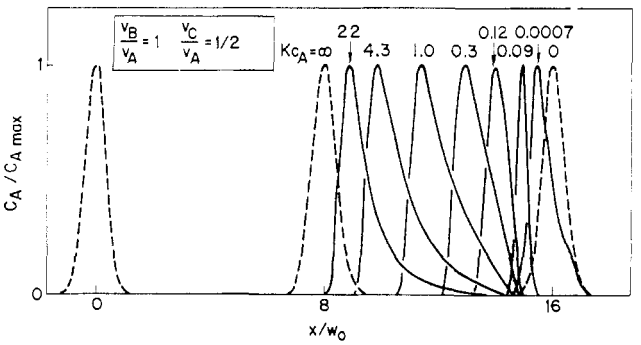

FIGURE 5: Normalized concentration profiles of A in the absence of diffusion with $v_A:v_B:v_C$ in the ratio 1:1:0.5. The amount of A loaded is small compared with the amount of B and the parameter which is relevant in determining the effective velocity of the A zone is Kc_A. Note the sharpening of the A zone when it travels near the rear edge of the much more abundant B zone ($Kc_A \approx 0.1$). The origin of this zone narrowing is discussed in section 1d.

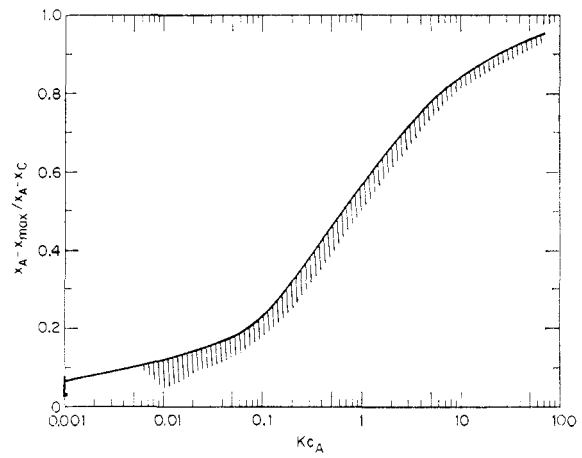

FIGURE 6: Summary of the results of Figure 5 (—) for $v_A = v_B > v_C$ and $l_A/l_B \ll 1$. x_{max} refers to the position of the labeled and least abundant species, A. The shaded area includes the results of simulated transport experiments in which the reactants are somewhat heterodromous. The labeled species is assumed to be A and the range of applicability is defined by $0.6 < (v_A - v_C)/(v_S - v_C) \leq 1.1$, where v_S is the velocity of the slower reactant. In this case the ordinate should be read as $(x_S - x_{max})/(x_S - x_C)$, where x_S is the position of the zone of the slower reactant in the absence of the faster reactant.

very small compared with that of B, and only c_A is monitored ($v_A = v_B$, $l_A/l_B \ll 1$).[5] Simulations corresponding to this limit are shown in Figure 5 for different values of Kc_A, *ie.*, as a function of the peak concentration of the least abundant species multiplied by K.

An inspection of the profiles shown in Figure 5 reveals two interesting features. First, the relevant parameter which characterizes the mobility of a complex zone is the product of K and the peak concentration of the labeled, least abundant species, c_A. The reason for the independence of the profiles on c_B is that immediately upon entering the gel, the A molecules in the complex zone retain a roughly equal number of B molecules with the remaining B's escaping with their usual velocity v_B. The complex zone contains approximately equal concentrations of A and B and its velocity depends on K as indicated for the equimolar limit of the section on principles. The second feature of interest is the narrowing which the A zone undergoes for small values of Kc_A, when the A zone finds itself traveling near the rear edge of the B zone. A molecules which escape to the front upon dissociation travel into a region of high B concentration where they are quickly complexed again, which leads to a sharpening of the front edge of the A zone. The rear edge is sharpened for the usual reason that complexes, upon dissociation, travel faster to rejoin the compound zone.

The results of the zone transport simulations like the ones shown in Figure 5 are summarized by the solid curve shown in Figure 6. In this figure diffusion effects are neglected but they have been found to play a negligible role (*cf.* Figure 4) in this case as well. The dependence of $\Delta x/\Delta x_{AC}$ shown by this curve is given to within a few per cent by the following expression

$$Kc_A = 0.61[(\Delta x_{AC}/\Delta x) - 1]^{-1.68} \quad (12)$$

or

$$\Delta x = \Delta x_{AC}/[1 + 0.75(Kc)^{-0.60}] \quad (13)$$

[5] By an argument analogous to the one employed to derive eq 5 and 6 one obtains for the case of rectangular zones $Kc_B' = [(\Delta x_{AC}/\Delta x) - 1]^{-1}$, where c_B' is the concentration of B in the complex zone, where it is approximately equal to c_A.

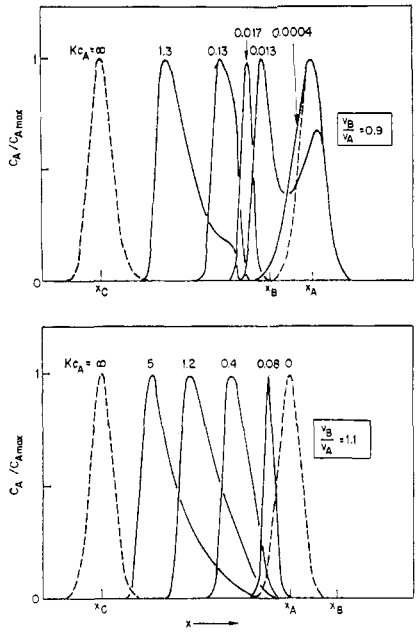

FIGURE 7: Normalized concentration profiles of the least abundant species A ($l_A \ll l_B$) with A and B approximately homodromous. The fractional retardations for these and similar situations all fall within the striped area shown below the solid curve in Figure 6. In the upper half of the figure the least abundant reactant A is 10% slower than B and in the lower half it is 10% faster. Note the zone narrowing when A travels close to the rear edge of the B zone.

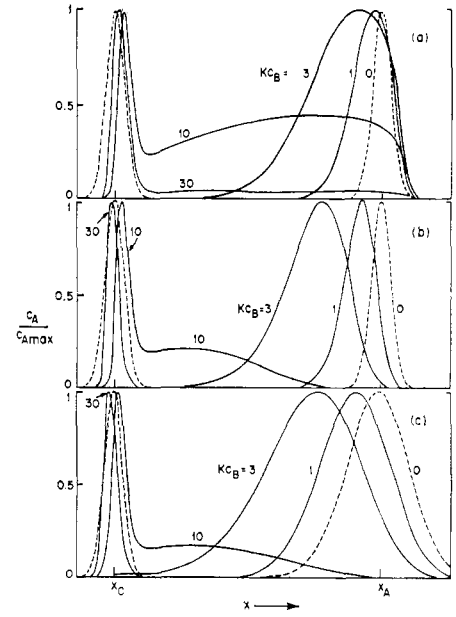

FIGURE 8: Normalized concentration profiles of the least abundant species A ($l_A \ll l_B$) traveling with a slower, abundant species B. In (a), A and B start simultaneously while in (b) and (c) B is given a headstart of $3w_0$, so that the A zone is made to travel through the B zone. The complex C is assumed to travel at the same velocity as B. Diffusion effects are neglected in (a) and (b). In (c) diffusion leads to a quadrupling of the A zone width with B and C diffusion considered negligible. The profiles clearly show the retardation of the fast species for Kc_B values less than 10. The retardations are seen to be greatly enhanced when the B zone is given a headstart ((b) and (c)). The presence of diffusion makes little difference to the retardation (c).

1e. Approximately Homodromous Reactants in the Low Concentration Limit. If the two reactants, A and B, are only approximately homodromous an analysis similar to that offered in the preceding section is still possible. The concentration profiles of the labeled, least abundant species (A) corresponding to v_A/v_B ratios of 0.9 and 1.1 are shown in Figure 7 ($l_A/l_B \ll 1$). The profiles retain most of the features of the corresponding homodromous case, including the zone narrowing for small values of Kc_A. When v_A exceeds v_B it is also possible to obtain profiles with maxima near the A and B positions. The results for this case fall within the stippled area in Figure 6. One can see that very little error is incurred by neglecting differences between v_A and v_B of the order of 10%.

2. Binding of Heterodromous Molecules

A fast molecule is generally retarded upon being bound to a slower one during a zone transport experiment. The retardation suffered by a zone of molecules upon passing through a zone of slower ones may be used to determine the strength of the interaction between heterodromous molecules. In this section are presented several simulated concentration profiles which illustrate the phenomenon. These results are summarized in figures which permit the determination of association constants once such experimental parameters as the zone retardation, zone width, and peak concentration have been determined.

In most of this section it will be assumed that the low concentration limit applies, *i.e.*, that the faster molecule (A) is the least abundant ($l_A \ll l_B$). The slower and abundant B zone will be perturbed to a negligible extent by the passage of the A zone through it. In order to measure the effects of the interaction on the A zone it is often necessary that the A zone profile, or at least its peak position, can be determined independently from B. This may be accomplished by differences in the optical properties of A and B or by labeling A, say by radioactivity or by fluorescence.

It is generally true that $v_A > v_B > v_C$, but since electrophoretic mobilities depend on molecular charge as well as size, the possibility that v_C exceeds v_B cannot be excluded. When A is much smaller than B, as would be the case for ligand binding to macromolecules, the velocity relationship is usually sufficiently well described by the approximation, $v_A > v_B = v_C$. In section 3a we will make use of this simplification and in section 3b it will be shown how these results may be extended to the general case ($v_A > c_B \neq v_C$).

2a. Retardation of the A Zone with $v_B = v_C$. Under these conditions the fraction of A molecules which are bound in the mixture present in the starting zone will determine the transport properties of A: when the fraction bound is small ($Kc_B \leq 3$) the A zone will be retarded from its position in the absence of B. When it is large ($Kc_B > 3$) A initially travels with B and constant leakage of A molecules from the forward edge leads to the appearance of a leading "shelf" in the concentration profiles of A. These characteristic features are illustrated in Figure 8a. The retardation of the peak of the A zone is an experimental parameter which can be measured conveniently and is found to be approximately proportional to Kc_Bw_B, *i.e.*, to the product of K and the number of B molecules present in the zone.

It is not surprising to find that the magnitude of the retardation of A is considerably larger if instead of loading A along with B, the A zone is made to pass completely through the B zone. In practice, this is achieved by loading B and, after permitting it to enter the gel, loading the A molecules. This procedure which is referred to as providing B with a headstart leads to retardations which are, for gaussian shaped zones,

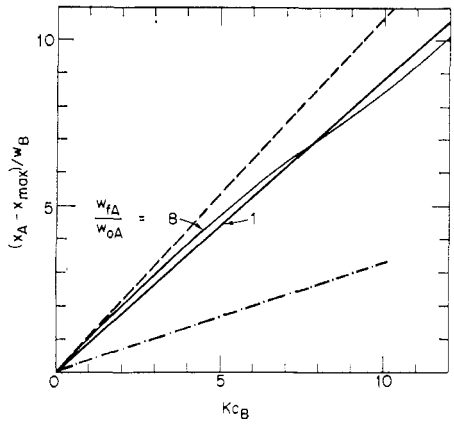

FIGURE 9: Summary of the retardations (as a fraction of the initial width) suffered by the fast species A as a result of interacting with a zone of slow and abundant species, B ($l_A \ll l_B$, $v_B = v_C$). The two solid curves show the results in the absence of diffusion, and in the presence of diffusion which leads to an eightfold increase in the width of the A zone during the run. The diffusion of B and C is considered negligible. The B zone was given a headstart of $3w_0$ in each case. The curve marked -·-·- corresponds to an experiment in which the A and B zones start simultaneously and diffusion is neglected. The retardations are only about one-third as great as were found in the corresponding headstart experiments. The dashed curve is the straight line relationship derived in Appendix 2 for heterodromous reactants with $v_B = v_C$ and guassian zone shapes (*cf.* eq A2-15). If, in evaluating the retardation one uses the centroid positions of the A zones instead of their peak positions, the results of the simulations (—) almost coincide with the dashed curve.

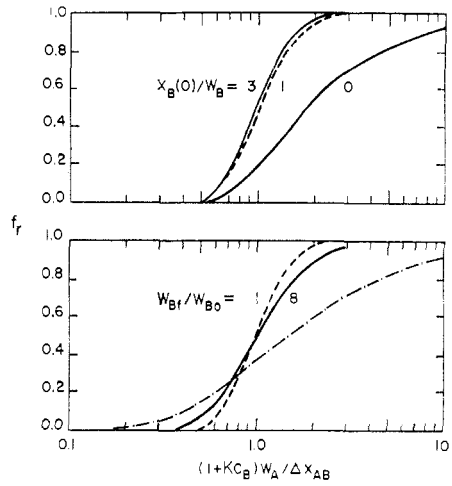

FIGURE 10: The fraction of A molecules (the fast and least abundant species) retained by the B zone ($l_A \ll l_B$, $v_A > v_B = v_C$) as a function of a dimensionless parameter combining K, c_B, Δx_{AB}, and w_A. The form of the parameter is that suggested by the derivation of eq A3-8. Note that as Kc_B increases and the length of the run is shortened, *i.e.*, as $\Delta x_{AB}/w_A$ decreases, the retained fraction f_r goes from 0 to 1. The steepness of the curve is greatest when the B zone is given a headstart, $x_B(0)$, of $3w_0$ or more (upper half of figure). The lower half of the figure shows the effect of diffusion of the A zone, which leads to an eightfold increase in the width of the A zone (- - -). The diffusion of B and C molecules is considered negligibly small. In these two curves the B zone is given a headstart of $3w_0$. The curve marked ····· finally corresponds to the theoretical expression derived for a rectangular zone model in the absence of diffusion (*cf.* eq A3-8).

approximately three times as great as in the absence of a headstart. This is illustrated in Figure 8b.

The relationship between retardation and binding can be understood readily if one considers the kinetics of rectangular zones. In Appendix 2 an expression for the retardation in terms of experimental parameters is derived. For gaussian zones and the case under discussion ($v_A > v_B = v_C$), this expression is given by eq A2-15 and is shown as a dashed line in Figure 9. The solid line shown for the diffusionless case in the same figure summarizes the results obtained in computer simulations and may be represented by the following equation.

$$Kc_B = 1.15\Delta x/w_B \qquad (14)$$

Figure 8c provides concentration profiles in the presence of headstart and diffusion which causes eightfold broadening of the A zone during the course of a run. The curves of Figure 9 show how the retardations corresponding to the profiles in Figure 8 depend on Kc_B. It is noteworthy that (1) the use of headstart increases the observed retardations and hence the accuracy of determining K considerably, (2) the diffusion effects are almost negligible, and (3) that the computer-simulated retardations are about 20% lower than those predicted by eq A2-15. This difference has its origin in the asymmetrical profiles of the A zones and the fact that we have defined retardations as the separation between x_A and the *peak* of the A zone profile, which is a convenient experimental parameter. If one uses the centroid of the A zone profiles a much closer agreement between the theoretical retardation and the simulated ones (*i.e.*, eq A2-15 and 14) is obtained.

Since the c_A profiles shown in Figure 8 exhibit maxima between x_B and x_A only as long as Kc_B is less than about 10, the retardation method for determining K is confined to such values. In any particular experiment c_B can of course be adjusted to fulfill this condition.

The magnitude of the headstart given to the B zone is irrelevant to retardation results given above as long as the A zone passes through all of the B zone. In practice, a headstart of $3w_B$ is sufficient to ensure this but larger headstarts are not detrimental except that they may increase the diffusion broadening slightly as the time required for running the gel will be longer.

2b. Retention of A by B Zone. In certain cases it may be simpler to measure the fraction of A molecules retained in the B zone rather than to determine the retardation of the A zone. This is particularly true if Kc_B is greater than 3 or if the determination of c_{Amax} is troublesome. Such a situation may arise if A is too dilute for optical scanning, or, alternatively, if A is radioactive but it is inconvenient to slice the gel. In this case the retained fraction may be obtained by making a single cut slightly ahead of the position of the B zone and measuring the ratio of activities in the two gel pieces.

In Appendix 3 the fraction of A molecules which is retained by the B zones (f_r) is obtained using the simplifying assumptions of rectangular zone shapes. When v_C is set equal to v_B the expression reduces (see eq A3-8) to

$$f_r = \exp\left[-\frac{1}{1 + Kc_B}\frac{\Delta x_{AB}}{w_A}\right] \qquad (15)$$

This equation suggests how f_r scales with Δx_{AB}, w_A, and c_B so that various experiments may be plotted together. Computer simulations for gaussian zones and including diffusion show that this scaling law holds under more realistic conditions. Figure 10 shows the dependence of f_r on $(1 + Kc_B)(w_A/\Delta x_{AB})$ under a variety of conditions. In determining f_r in these simulations, it was defined arbitrarily as the fraction of A molecules which has traveled no further than $x_B + 1.5w_B$ during a run

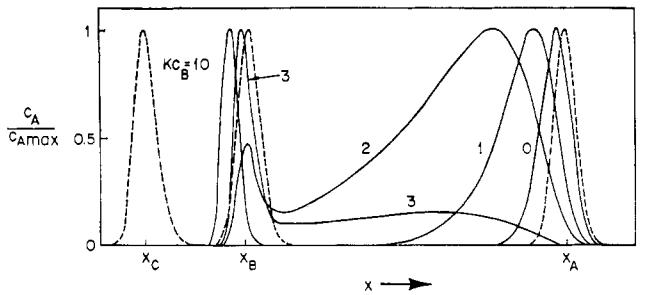

FIGURE 11: Normalized concentration profiles of the fastest species A following a zone transport experiment in the presence of B, the B zone having been given a headstart. $v_B - v_C = {}^1/_3(v_A - v_B)$ and $l_A \ll l_B$. Note that for Kc_B values greater than 3, for which v_B exceeds v_{AB} (see Appendix 3) the A zone suffers a "reflection" for the length of experiment simulated here, *i.e.*, for $\Delta x_{AB} = 12w_A$. For a sufficiently long experiment the A molecules would of course eventually penetrate the B zone. These profiles differ from those in Figure 8 in that $v_B \neq v_C$.

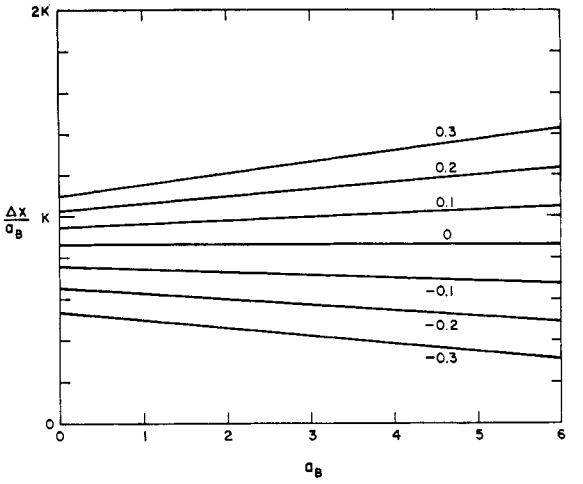

FIGURE 12: The reduced retardation $\Delta x/a_B$ suffered by an A zone upon passing through a B zone of area a_B for different ratios of $\alpha = (v_B - v_C)/(v_A - v_B)$. a_B is the area under the concentration profile of the B zone obtained by scanning the gel along its length. The lines shown in the figure represent fits to computer simulated experiments with $l_A/l_B \ll 1$ in the absence of diffusion with $|\alpha| \leqq 0.3$. The resulting family of lines is represented by eq 22. In actual experiments in which K is unknown a protocol like the one used in Figure 15 is employed to determine K.

which separates the (unbound) A zone and the B zone by a distance Δx_{AB}.

The upper part of the figure shows the effect of giving the B zone a headstart ($\Delta x_B(0)$) and the lower part illustrates the small effect of diffusion of the A zone upon the results. Thus f_r may be obtained simply by cutting the gel into two segments at $1.5w_B$ beyond x_B and determining the total counts (or OD units or fluorescence yield) in each segment.

Instead of using the graphical solution discussed above, one may represent the retained fraction as defined above, in the diffusionless case and in the presence of a headstart of $2w_B$ or more, by the following equations obtained by fitting computer simulations. Their accuracy is a few per cent in f_r.

$$Kc_B = 0.95(\Delta x_{AB}/w_A)(f_r^{-1} - 1)^{-0.155} - 1 \qquad (16)$$

or

$$f_r^{-1} = 1 + [1.05(Kc_B + 1)(w_A/\Delta x_{AB})]^{-6.45} \qquad (17)$$

2c. Retardation of the A Zone with $v_B \neq v_C$. In this, the most general case of heterodromous reactants, v_C may be greater or smaller the v_B. As can be guessed from the retardation formulas for rectangular zones derived in Appendix 2, the retardation (Δx) of the fastest reactant may still be used to evaluate K but this value will be a function of $\alpha = \Delta v_{BC}/\Delta v_{AB}$ as well as Δx and the width and concentration of the B zone ($\Delta v_{BC} = v_B - v_C$, etc.). Fortunately it is not necessary to know v_C or α to determine K, if the retardation of the A zone is measured at several concentrations of B as will be seen below. The concentration in the A zone will be assumed small compared to that in the B zone, as in the preceding sections.

In Appendix 2 it is shown that for rectangular zones

$$\frac{\Delta x}{a_B} = \frac{1 + \alpha}{1 - \alpha K a_B/w_B} K \qquad (18)$$

where $a_B = c_B w_B$ is the area of the rectangular B zone. Note that α may be positive or negative.

According to eq 18 a plot of $\Delta x/a_B$ *vs.* a_B yields a curve which approximates a straight line as long as α is small compared to unity and its intercept (I_r) and initial slope (S_r) are given by

$$I_r = (1 + \alpha)K \qquad (19)$$

$$S_r = \alpha(1 + \alpha)K^2/w_B \qquad (20)$$

If α is not too large, one obtains from these equations

$$\alpha = S_r w_B/I_r^2 \qquad (21)$$

In principle, therefore, one may use eq 18 and 21 to evaluate K.

These considerations for rectangular zones indicate how retardation experiments for gaussian zones should be analyzed. The computer-simulated retardations ($\Delta x/a_B$) for a number of positive and negative values of α (*cf.* Figure 11) were plotted against a_B as indicated in Figure 12. The points corresponding to particular values of α were fitted by curves with the same functional form as eq 18 to obtain expressions for their intercepts (I) and slopes (S) in terms of effective values for α and K. The family of curves corresponding to $-0.3 < \alpha < 0.3$ could all be fitted by the following formula for K in terms of experimental parameters: ($I = \lim_{a_B \to 0}(\Delta x/a_B)$, $S = \partial/\partial a_B(\Delta x/a_B)$)

$$K = 1.17I(1 - 5Sw_B/I^2) \qquad (22)$$

The semiempirical eq 22 yields K with an error of less than a few per cent as long as $|5Sw_B/I^2|$ is less than 0.15, which corresponds to $|\alpha| < 0.3$.

When $\alpha = 0$, the values of $\Delta x/a_B$ are found to be independent of a_B, *i.e.*, S is zero and

$$K = 1.17\Delta x/a_B \qquad (23)$$

Recalling that for gaussian zones $a_B = 1.06c_B w_B$, eq 23 could also be written $Kc_B = 1.10\Delta x/w_B$ which differs only slightly from the computer-simulated results for $v_A > v_B = v_C$ which are given in Figure 9 and eq 14.

Since one cannot be certain whether and by how much v_B and v_C differ in any particular retardation experiment, one should proceed as follows. Determine Δx for various values of a_B to achieve retardations up to about $2w_B$. If the corresponding $\Delta x/a_B$ values show no systematic trend with a_B, it may safely be concluded that $v_B \approx v_C$ and eq 14 should be used to evaluate K. If $\Delta x/a_B$ shows a monotonic dependence

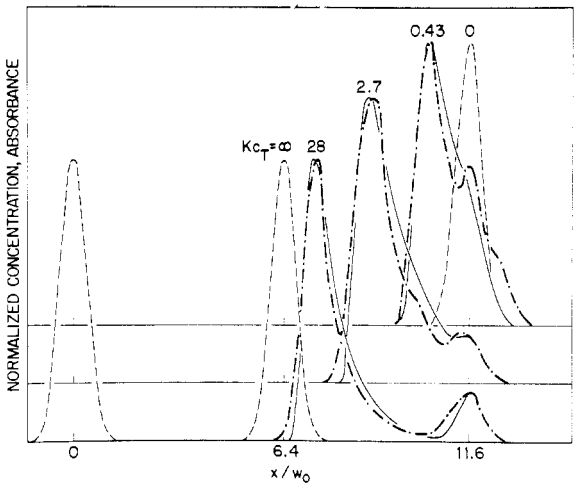

FIGURE 13: A comparison of the total concentration profiles determined spectrophotometrically with simulated profiles in the case of the electrophoresis of nominally stoichiometrically equal amounts of $tRNA^{Phe}$ and $tRNA^{Glu}$. The dashed curve, $Kc_T = 0$, is the experimental profiles of a single species. The curves –·–·– show the experimental profiles with increasing concentrations of the equimolar mixtures. The solid curves are computer simulated profiles assuming a single value for the association constant, the experimentally observed peak concentration, and a velocity of the complex equal to 0.55 of that of the monomeric tRNAs. To improve the fit of the simulated profiles it was assumed that the stoichiometry of loading was violated by up to 15%. See section 4a for experimental conditions.

on a_B, a plot is made to determine the slope $S = \partial(\Delta x/a_B)/\partial a_B$ and the intercept I, and eq (22) is used to determine K. The various $\Delta x/a_B$ values should of course be weighted according to their experimental uncertainties.

The power of the protocol given above lies in the fact that while the linear correction factor in eq (14) was derived for values of α between ± 0.3, the K one obtains by the use of eq 14 is in error by less than 40% when the correction factor Sw_B/I^2 is as large as 0.5, corresponding to $|\alpha| \sim 0.7$.

As is indicated in Appendix 3, situations in which v_C differs from v_B are better approached by the retardation method than by the retention method discussed in the preceding section.

3. Comparisons between Theory and Experiments

In this section experimental results which demonstrate the validity of the computer simulations of gel electrophoresis of interacting molecules are given. The three examples presented here also illustrate some of the experimental techniques[6] which permit the determination of binding constants with the aid of the theory presented in the preceding sections.

3a. Complex Formation of tRNA Molecules. It has been pointed out (Eisinger, 1971) that pairs of tRNA molecules whose anticodon triplets are complementary to each other (*e.g.*, $tRNA^{Phe}$ and $tRNA^{Glu}$) form complexes with association constants of the order of 10^6 M^{-1}. In as much as all amino acid specific tRNAs have comparable gel electrophoretic mobilities this interaction illustrates the pseudodimerization limit.

Figure 13 shows absorbance profiles following the electrophoresis of nominally equimolar mixtures of $tRNA^{Phe}$ and $tRNA^{Glu}$.[7] The figure also shows the profile of $tRNA^{Phe}$ in the absence of $tRNA^{Glu}$. When both tRNAs were loaded on the gel and run for the same length of time the total concentration peak moved to the left, and for the three profiles shown the observed peak absorbances at 260 nm were 0.019, 0.10, and 0.83, respectively, corresponding to total tRNA concentrations of 0.08, 0.46, and 3.8 μM, respectively. If one assumes that the dimer travels with 0.55 of the monomer velocity, the three experimental curves can be fitted quite well by using $Kc_T = 0.43$, 2.7, and 28. Within the experimental errors these three parameters are seen to be in the same ratio as the observed total monomer concentrations given above and one obtains a value of $K = 6 \times 10^6$ M^{-1} for the association constant at 3° at neutral pH. The simulated profiles were obtained without diffusion terms since the zone widths were found to broaden by negligible amounts during the time taken for electrophoresis. Small deviations for nonstoichiometric loading were taken into account. It is gratifying that the single association constant given above could account for concentration profiles of three zones the concentration of which ranges over a factor of 40.

To analyze this experiment without benefit of a computer one proceeds as follows. Having determined the position of the complex peak at as many values of c_T as feasible, values for $(x_A - x)/\Delta x_{AC} = \Delta x/\Delta x_{AC}$ are listed assuming different values of v_C/v_A ($\Delta x_{AC} = [1 - (v_C/v_A)]x_A$). For each assumed value of v_C/v_A one obtains a set of values of Kc_T from the set of values of $\Delta x/\Delta x_{AC}$ by using the solid curve of Figure 5 (or, alternatively, eq 10).[8] Since c_T is known, a set of values of K may be obtained by simple division. The consistency of these K values with each other is the criterion by which the correct v_C/v_A is chosen. In Table I we have listed the K values corresponding to experimental Δx and c_T values for three assumptions for v_C/v_A. It is clear that $v_C/v_A = 0.525$ gives the most consistent set of K values and one obtains $K = (5 \pm 2) \times 10^6$ M^{-1}, where the error is estimated from the uncertainty in the individual values of K caused by experimental errors in c_T and Δx.

3b. tRNA–Oligomer Binding. It has recently been pointed out that the secondary and tertiary structure of RNA molecules with known primary sequence can be investigated by measuring the binding of oligonucleotides with base sequences which are complementary to short stretches of the RNA in question (Uhlenbeck *et al.*, 1970; Uhlenbeck, 1972). While the strength of the binding is sensitive to several parameters (*e.g.*, the base sequences and structure of the oligomer and the RNA), no binding is observed if the RNA region involved is double stranded. Most of these studies have made use of equilibrium dialysis which suffers from the disadvantage that it requires high ionic strength and becomes prohibitively slow

[6] Polyacrylamide gels (7.5–10% acrylamide with 4% bisacrylamide) were formed in a conventional manner inside quartz capillary tubes (i.d. 2.8 mm, o.d. 7 mm). Water was layered on the gel before polymerization to provide a flat gel meniscus. Tris buffers (pH 7.5–8) were used except in the chymotrypsin experiments for which the buffer was KH_2PO_4 with NaOH adjusted to pH 7.0 and ionic strength 0.4 M. All molecules were loaded in 10% sucrose with the aid of microliter syringes. The gels were run in a commercial cell holder with the lower reservoir buffer reservoir generally stirred and cooled. Power dissipation was always less than 0.4 W per gel (12) corresponding to a temperature rise within the gel of 1°. Concentration profiles of tritiated molecules are obtained by slicing the gel after removal from the capillary tube into 1–2-mm slices. After adding 0.2 ml of NCS–H_2O (9:1) (Amersham-Searle) the slices were allowed to remain at room temperature overnight and a counting cocktail was added. Counting errors were less than 1% at peak concentrations.

[7] $tRNA^{Phe}$ (yeast) was purchased from the Boehringer Corp., and $tRNA^{Glu}$ (*E. coli*) was kindly supplied by the Oak Ridge National Laboratory tRNA project.

[8] The fact that this experiment employed a headstart of w_B, rather than $2w_B$ or more, affects K by a negligible amount (*cf.* Figure 11a).

TABLE I: Association Constants for $tRNA^{Phe}$–$tRNA^{Glu}$ Binding Derived from the Observed Retardations at Different Concentrations with the Aid of Figure 4.[a]

	v_C/v_A					
	0.5		0.525		0.6	
c_T (10^{-6} M)	$\Delta x/\Delta x_{AC}$	K 10^6 (M^{-1})	$\Delta x/\Delta x_{AC}$	K 10^6 (M^{-1})	$\Delta x/\Delta x_{AC}$	K (10^6 M^{-1})
0.08	0.20	4.6	0.21	5.0	0.25	6.2
0.46	0.49	4.0	0.52	5.0	0.62	9.1
3.8	0.77	3.3	0.81	4.9	0.97	>130

[a] Three different assumptions for the velocity ratio v_C/v_A were employed. The consistency of K for three widely different peak concentrations (c_T) indicates that $v_C/v_A = 0.525$.

for oligomers longer than tetramers. In this section the determination of the association constant of AUGA binding to $tRNA^{fMet}$ (*E. coli*) is described and comparisons are offered between the experimental and simulated AUGA profiles.[9]

From the gel electrophoresis of $tRNA^{fMet}$ and AUGA alone it was shown that the tetramer travels 1.8 times faster than the tRNA and that its diffusion constant is 1.8 times greater. Neither diffusion is very serious: after traveling a distance of 2 cm the width of the tRNA zone had increased from 2 to 3 mm. The concentration profiles of the (tritiated) tetramer and tRNA zones were measured by slicing and counting and by uv absorption, respectively. The specific activity of the AUGA was sufficiently high to ensure that the molarity of AUGA zones could be made much smaller than the tRNA molarity. The low concentration limit of the binding equation was therefore appropriate. $tRNA^{fMet}$ (2.2 *A*) was loaded on a gel, and after 30 min it had received a headstart of w_0 (here 2 mm). The tetramer was then loaded on the same gel in which the tRNA load was ten times smaller or was omitted entirely. Following electrophoresis the concentration profiles shown in Figure 14 were obtained. The figure also shows three simulated concentration profiles calculated with the assumptions that $Kc_{Bmax} = 0.5$, 1.0, and 1.5. The best fit was obtained with $Kc_{Bmax} = 1.0$. From the peak absorption of the tRNA zone and the optical effective path length of the gel in the capillary, $c_{tRNAmax}$ was calculated to be 1.5×10^{-4} M. The association constant is therefore 7×10^3 M^{-1} with an estimated error of about 30%. This value was obtained at 0° at pH 7.5 in the presence of 0.01 M $MgCl_2$ and 0.4 M NaCl.

The same experiment can of course be analyzed without using computer simulation by noting that the retardation, Δx_{AUGA}, is 0.9 w_{tRNA}. If it is assumed that the electrophoretic mobility of the tRNA–AUGA complex is almost the same as that of tRNA, eq 14 is applicable and K is given by $1.0/c_{tRNA} = 7 \times 10^3$ M^{-1}, the same value as was obtained in the preceding paragraph.

Uhlenbeck measured the binding of the same tetramer to $tRNA^{fMet}$ in 1 M NaCl by equilibrium dialysis and obtained $K = 13.5 \times 10^4$ M^{-1}. He also estimated the dependence of K on ionic strength for AUCA binding to $tRNA^{Tyr}$ and found

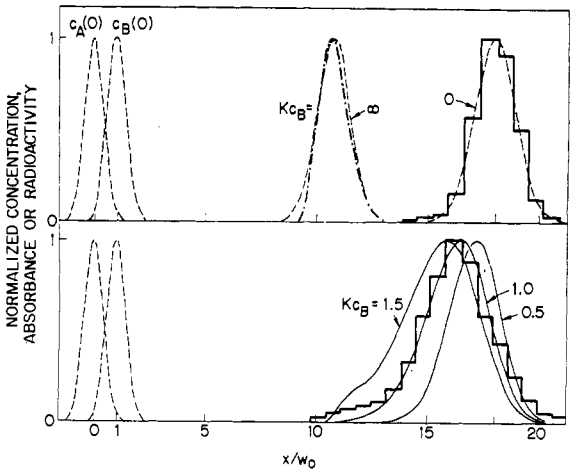

FIGURE 14: Determination of the association constant for AUGA binding to $tRNA^{fMet}$. The upper part of the figure shows the concentration profiles of $tRNA^{fMet}$ and the tetramer, each run in the absence of the other. The curve (–·–·–) for the tRNA was obtained by scanning the gel spectrophotometrically, (– – –) representing the final gaussian zone which was used for the computer simulation. It includes some diffusion broadening. The upper histogram is the AUGA profile obtained by slicing the gel and counting. The dashed curve is the gaussian profile used in the computer simulations. The histogram in the lower part of the figure represents the experimental AUGA profile after having been run in the presence of $tRNA^{fMet}$. The tRNA had been given a headstart to maximize the observable retardation. The three curves in the lower part of the figure represent computer-simulated profiles for different assumptions of Kc_{tRNA}. The observed value of c_{tRNA} at its maximum was 1.5×10^{-4} M, from which K is 7×10^3 M^{-1} (see section 4b).

that K at 0.4 M NaCl is two-thirds of its value of 1 M NaCl. If one assumes the same ionic strength dependence for the binding of AUGA to $tRNA^{fMet}$, the dialysis value of K under the conditions used by us would be 10×10^3 M^{-1}, which is consistent with the value obtained by gel electrophoresis.

3c. Binding of Proflavine to δ-Chymotrypsin. Proflavine is an inhibitor of δ-chymotrypsin (ChT) whose binding to the active site of δ- and α-chymotrypsin has been investigated by various methods and under various techniques (Brandt *et al.*, 1967; Fersht and Requena, 1971). We used this reaction to illustrate the most general case of heterodromous reactant binding ($v_A > v_B \neq v_C$).

Samples of δ-chymotrypsin solutions (5 or 10 μl) of various concentrations were loaded on 7.5% polyacrylamide gels.[10] At pH 7.0 the enzyme is an anion which traveled at a rate of about 0.15 cm/hr. After the chymotrypsin zones had traveled a distance of about 0.7 cm into the gels, 10-μl aliquots of proflavine solutions whose molarity was much lower than that of the chymotrypsin solutions were loaded on each of these gels as well as on two gels containing no chymotrypsin. Since proflavine is a cation at neutral pH, the polarity of the applied voltage had to be reversed to permit it to enter the gels. This caused the chymotrypsin zones to reverse their direction of travel and to collide with the proflavine zones, but since the proflavine zones traveled at 12 times the velocity

[9] $tRNA^{fMet}$ (*E. coli*) was kindly supplied by the Oak Ridge National Laboratory tRNA project. ^3H-labeled AUGA was the gift of O. C. Uhlenbeck, who had synthesized this tetramer. The molar extinction coefficient of $tRNA^{fMet}$ was taken (Blum *et al.*, 1972) to be 5.4×10^5.

[10] Bovine pancreatic δ-chymotrypsin (Worthington) and proflavine (National Biochemicals) were used without further purification. The enzyme solutions were kept cold or frozen at pH 3 until ready to load on the gel or added to the titration samples. Activity was determined before and after experiments to assure negligible autolysis. Enzyme concentrations were determined spectrophotometrically using $\epsilon(282) = 5 \times 10^4$ for the molar extinction coefficient.

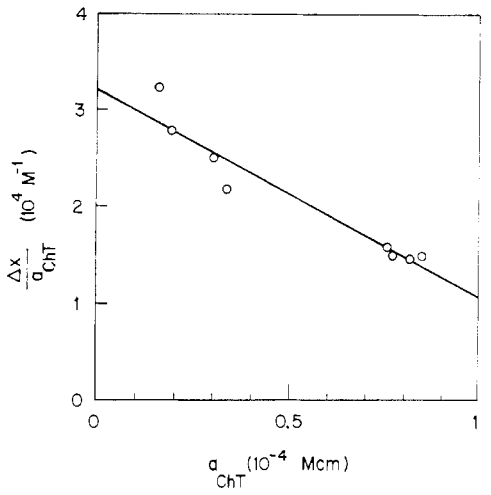

FIGURE 15: Proflavine zones were retarded by distances (Δx) between 0.6 and 1.5 cm upon passing through chymotrypsin zones of different concentrations. The zone areas a_{ChT} are a measure the amount of enzyme encountered by the proflavine zones which were always dilute compared to the δ-chymotrypsin zones. The line shown is a fit to the experimental points and its slope (2.1×10^8 cm^{-1}) and intercept (3.2×10^4 M^{-1}) where substituted in eq 22 to obtain K.

of the chymotrypsin zones, the proflavine zones in the various gels were between 0.8 and 2.3 cm into the gel when the chymotrypsin zones had traveled about 0.2 cm back toward the gel meniscus. The gels were then scanned spectrophotometrically in the visible region to determine the dye profiles and in the ultraviolet region to obtain the enzyme profiles. From these profile values for Δx, a_{ChT} and $\Delta x/a_{ChT}$ were calculated and $\Delta x/a_{ChT}$ was plotted against a_{ChT} as shown in Figure 15. The slope and intercept of this plot were then used to calculate $K = 4.8 \times 10^4$ M^{-1} from eq 22. The error is estimated to be about 30%. The negative slope of the line shown in Figure 15 indicates that the effective α value is negative and of the order of -0.3. This means that the proflavine–δ-chymotrypsin complex is a cation, and the following ratio of zone velocities was obtained under the conditions of the experiment v_{Pro}: $v_{ChT}:v_{Pro-ChT} \approx 1:-0.08:0.3$.

The binding constant was also determined by fitting the absorbance changes at 470 nm of a series of titration samples to the binding equation by a computer program which minimized the sum of the root mean square deviations to determine optimum values of K and the limiting values of the absorbance at 470 nm for zero and infinite δ-chymotrypsin concentrations. The proflavine molarity of the nine samples used was 1.35 μM, and the δ-chymotrypsin molarity was varied between 0 and 2 mM. The result was $K = 3.5 \times 10^4$ M^{-1} and is consistent with the value given in the preceding paragraph. Both values are in approximate agreement with values in the literature for δ- and α-chymotrypsin and somewhat similar conditions of pH and ionic strength (Brandt *et al.*, 1967; Fersht and Requena, 1971).

4. Summary and Discussion

The results the computer simulated transport experiments obtained in the preceding sections are summarized in Table II. This table contains expressions for Kc in terms of observable parameters from retardation and retention experiments. The table gives solutions for rectangular zones as well as gaussian ones, the former being included merely for heuristic reasons: they can be derived analytically and illustrate the relationships

TABLE II: Summary of Relationships between Binding Constants and Observable Parameter for Rectangular and Gaussian Zones.[a]

Reactants	Loading $v_A:v_B:v_C$	Loading I_A/I_B	Kc Measured from Retardation, Δx		Kc Measured from Retained Fraction f_r	
			Rectangular Zones	Gaussian Zones	Rectangular Zones	Gaussian Zones
Homodromous[e]	$v_A = v_B > v_C$	$\ll 1$	$Kc_A = (\Delta x_{AC}/\Delta x - 1)^{-1}$	$Kc_A = 0.61(\Delta x_{AC}/\Delta x - 1)^{-1.68}$		
		$= 1$	$Kc_T = \dfrac{1 + \sqrt{(1 - \Delta x/\Delta x_{AC})^2 + 1}}{(1 - \Delta x/\Delta x_{AC})^2}$	$Kc_T = 2.2\left(\dfrac{\Delta x_{AC}}{\Delta x} - 1\right)^{-1.35}$		
Heterodromous[f]	$v_A > v_B = v_C$	$\ll 1$	$Kc_B = \Delta x/w_B$	$Kc_B = 1.15(\Delta x/w_B)$ $K = 1.08(\Delta x/a_B)$	$Kc_B = -(\Delta x_{AB}/w_A \ln f_r + 1)^d$	$Kc_B = 0.95\dfrac{\Delta x_{AB}}{w_A}(f_r^{-1} - 1)^{-0.155} - 1$
	$v_A > v_B \neq v_C$	$\ll 1$	$Kc_B = \Delta x/w_B[1 + \alpha(1 + \Delta x/w_B)]^{-1}$	$K = 1.17(1 - 5Sw_B/I^2)^c$	$Kc_B = \dfrac{x_{AB}/w_A \ln f_r + 1}{\alpha\Delta x_{AB}/w_A \ln f_r - 1}^{b,d}$	

[a] Only the expressions for gaussian zones or their graphical equivalents presented in the figures of this paper should be used in analyzing experiments. Examples for homodromous reactants are dimerization or pseudodimerization reactions and heterodromous reactants are exemplified by ligand binding reactions. [b] Valid only for $Kc_B > \alpha$ ($\alpha = \Delta v_{BC}/\Delta v_{AB}$). [c] $I = \lim_{a_B \to 0} \Delta x/a_B$, $S = (\partial/\partial a_B)(\Delta x/a_B)$; see section 3c. [d] Valid only for $\Delta x_{AB}/w_A > |\ln f_r|$. [e] No headstart. [f] B zone has headstart of $3w_B$ or more.

under restricted conditions. While the formulas given in the table do not allow for diffusion, it was shown in the preceding sections that for the parametrization employed here diffusion plays a negligible role.

Homodromous reactants can only be studied by retardation experiments while heterodromous reactants should generally be approached by retardation experiments with A being given a headstart of at least two zone widths. In special situations retention experiments may be more convenient. This is particularly advantageous in experiments for which A is radioactive since it may obviate the need for slicing the gel following electrophoresis. A single cut at $x_B + 1.5w_B$ is all that is needed.

The transport properties of interacting molecules in experiments using moving boundaries instead of zones are described by the same differential equations (eq 3a–c). The solutions of the equations for these two cases differ only because of differing initial boundary conditions. In fact, it has been pointed out (Bethune and Kegeles, 1961) that the profiles of a moving boundary and the integral of a moving zone are identical. It is clear therefore that most of the experimental protocols presented here can be adapted to moving boundary experiments in a straightforward manner but they would suffer from two experimental disadvantages. Positions of boundaries are defined by maximum concentration gradients rather than by concentration maxima, and since a constant supply of the interacting molecules must be maintained a larger amount of material is required. For the retention experiments, on the other hand, no analogous moving boundary protocol exists, since these depend for their analysis on dividing a bolus (of finite size) into two fractions.

While the graphical solutions and formulas given here are derived for gaussian zones they are quite insensitive to the precise zone shape. Retardation experiments with headstart are in fact best analyzed by plotting Δx *vs.* a_B, in which case the shape of the B zone is immaterial. The shape of the B zone in such cases only enters in the correction term which appears when $v_B \neq v_C$, since it is proportional to w_B. An approximate value of w_B is sufficient.

In an actual experimental situation the nature of the interacting molecules will generally suggest if one is dealing with homodromous or heterodromous reactants but an experimental test, preferably in polyacrylamide gels of different constitutions will help in finding a matrix and buffer which maximizes the difference between v_A and v_B. The method of choice is then a retardation experiment with headstart. If it is impossible to find a suitable matrix in which v_A exceeds v_B by more than 10 or 20%, and A and B have comparable molecular weights they may be treated as homodromous reactants.

In headstart experiments it is of course not necessary to allow the B zone to migrate into the gel. It could be introduced by other means such as by linking the B molecules to the matrix. The retardation formulas given above continue to hold as long as the electrophoretic properties of free A molecules within the B zone remain unchanged.

The magnitudes of binding constants which may be studied by these techniques cover an enormous range. The lower limit of K for which the method may be used is of the order of c_S^{-1} where c_S is the molarity of the most concentrated solution which can be prepared. At the high end the limit for a retardation experiment is given by one's ability to detect the least abundant species (A) and depends therefore on the diameter of the gel and the specific activity of A, if it is detected by its radioactivity, for instance.

Finally it should be noted that the protocols presented in this paper (*cf.* Table II) permit the elucidation without recourse to a computer of the associative properties of a large fraction of binary systems encountered by biochemists.

5. Acknowledgments

We wish to thank Nancy Gross for her expert technical assistance and George Robillard for his help with the δ-chymotrypsin experiments.

Appendix 1

Numerical Integration of the Transport Equations. The transport of two reversibly interacting molecules (A,B) in the presence of diffusion is described by the differential eq 3a–c. The solutions at any time t, $c_{A,B,C}(x,t)$, depend only on the initial conditions $c_{A,B,C}(x,0)$ and may in principle be obtained by direct integration. Equations 3a–c are, however, not integrable in a closed form, but, by using finite difference equations to approximate them, the integration can be carried out numerically. For this purpose it is assumed that the length of the gel is divided into N slices of width Δx and that the time required for the A zone to traverse the length of the gel is divided into N intervals of duration Δt. Starting with initial concentration profiles of A, B, and C, the numerical integration proceeds as follows.

First x is held fixed and as t is increased by Δt, the variations in terms 3 and 4 of the right sides of eq 3a–c are evaluated throughout the gel. Then t is held fixed and the transport and diffusion terms (1 and 2 of the right sides) are evaluated. A moves Δx while B and C move increments 0 or $\pm\Delta x$ depending on their velocities relative to A and the time elapsed since their last advance. For example, if $D = 0$ and $v_B/v_A = {}^1/_3$ the entire profile of B is advanced by Δx every third cycle of numerical integration.

In addition, diffusion and heterogeneity[11] are taken into account by decreasing the concentration of A, B, or C at a point x by δc and increasing the concentration at $x \pm \Delta x$ by $\delta c/2$. The magnitude of δc depends on the diffusivity D and on N.

For sufficiently large N this procedure approximates exact solutions for any k_f and k_r. In cases for which k_f and k_r are not large enough for equilibrium to be established among A, B, and C in a time interval $(\Delta x/w)\Delta t$, the solutions will depend on both k_f and k_r. If, however, equilibrium *is* reestablished during this time interval only the ratio $k_f/k_r = K$ enters into the solutions. In order to test the influence of a finite N on the final concentration profiles, we used $N/w_0 =$ 1.25, 2.5, 5, 10, and 20 and permitted the fastest zone to travel a distance of $20w_0$ under a variety of loading and binding conditions. For $N/w_0 \geq 5$ the equilibrium constant measured from the simulated profiles using one of the protocols given in this paper deviated only a few per cent from the value used for the computation. For $N/w_0 = 5$ the effect of finite Δx was visible on the profiles when they were narrow ($w \approx w_0$) but not objectionably so. For $N/w_0 \geq 10$ all profiles appeared smooth within the precision of the plotter. Since

[11] Heterogeneity of the mobility may be simulated by making the diffusion coefficient D in eq 3a–c increase as the square root of the elapsed time. This produces a width which increases linearly with time or distance traveled. We have found that the zone broadening of certain samples (*e.g.*, tRNA) is well simulated by this method, but we have not used such samples in binding experiments. It should be noted that those expressions in Table II which depend only on the measurement of an area or a peak position are unchanged in the presence of a heterogeneous mobility.

the computation time depends on N^2, the smallest practical value, $N/w_0 = 5$, was used throughout for simulated profiles.[12]

Appendix 2

Retardation of a Fast Zone by a Slower Zone. It is assumed that A and B zones have sharp boundaries with widths and velocities w_A, w_B, and v_A, v_B and that $v_A > v_B > v_C$.

When an A zone passes through a B zone and A and B are in rapid equilibrium with their complex C, the A zone will be retarded by a distance

$$\Delta x = (v_A - v_{AB})t_{AB} \qquad \text{(A2-1)}$$

where v_{AB} is the velocity of the A zone within the B zone and t_{AB} is the time required for the A zone to pass through the B zone. Now

$$v_{AB} = fv_C + (1 - f)v_A \qquad \text{(A2-2)}$$

and the fractions of A molecules which are free and bound while in the B zone are, in the low concentration limit ($l_A \ll l_B$), given by

$$f = Kc_B/(1 + Kc_B) \qquad \text{(A2-3)}$$

and

$$1 - f = 1/(1 + Kc_B) \qquad \text{(A2-4)}$$

Equation A2-2 may therefore be written as

$$v_{AB} = (v_A + Kc_Bv_C)/(1 + Kc_B) \qquad \text{(A2-5)}$$

Since

$$t_{AB} = w_B/(v_{AB} - v_B) \qquad \text{(A2-6)}$$

the retardation (eq A2-1) may be written as

$$\Delta x = [(v_A - v_{AB})/(v_{AB} - v_B)]w_B \qquad \text{(A2-7)}$$

Using (A2-5) in (A2-7) one obtains

$$\Delta x = [(1 + \alpha)/(1 - \alpha Kc_B)]Kc_Bw_B \qquad \text{(A2-8)}$$

where we have written $\alpha = \Delta v_{BC}/\Delta v_{AB}$. Equation A2-8 may be solved for Kc_B.

$$Kc_B = \frac{\Delta x/w_B}{1 + \alpha(1 + \Delta x/w_B)} \qquad \text{(A2-9)}$$

These equations hold as long as $\alpha Kc_B < 1$.

If $v_B = v_C$, eq A2-9 simplifies to

$$Kc_B = \Delta x/w_B \qquad \text{(A2-10)}$$

While this equation was derived for rectangular zones, its validity may be extended to B zones with arbitrary profiles by considering them as consisting of many rectangular zones of infinitesimal widths. One may then write

$$\Delta x = K\int_0^\infty c_B(x)dx = Ka_B \qquad \text{(A2-11)}$$

where a_B is the area of the B zone in mcm and Δx is the retardation in cm, *i.e.*

$$K = \Delta x/a_B \qquad \text{(A2-12)}$$

A plot of Δx *vs.* a_B should yield a straight line through the origin with a slope of K (M^{-1}).

In the computer simulations we have used gaussian line shapes so that the following relationships between a_B, c_{Bmax}, and w_B hold (w is the width at half-maximum)

$$c_B(x) = c_{Bmax}\exp\{-4(\ln 2)x^2/w_B^2\} \qquad \text{(A2-13)}$$

$$a_B = \frac{\sqrt{\pi}}{2\sqrt{\ln 2}}w_Bc_{Bmax} = 1.06w_Bc_{Bmax} \qquad \text{(A2-14)}$$

For gaussian B zones, therefore, eq A2-11 becomes

$$K = 0.94\Delta x/c_Bw_B \qquad \text{(A2-15)}$$

This is the equation of the dashed line shown in Figure 10.

Appendix 3

Retardation of Fast Molecules by a Slow Zone. Assume both A and B zones have sharp boundaries and that w_A, w_B and v_A, v_B are their widths and velocities. The complex C is assumed to have velocity v_C and $v_A > v_B > v_C$.

A molecules begin to escape from the B zone at a time when the forward edges of the two zones coincide. The rate of escape in the forward direction is proportional to the difference of velocities of A molecules inside and outside the B zone. The fraction of A molecules escaping in an infinitesimal time interval is

$$dc_A/c_A = -[(v_{AB} - v_B)/w_A]dt \qquad \text{(A3-1)}$$

where v_{AB} is the velocity of the A zone within the B zone. Integrating (A-31) one finds that the fraction of A molecules which have escaped in time t' is

$$c_A/c_{A0} = 1 - \exp(-(v_{AB} - v_B)/w_A)t' \qquad \text{(A3-2)}$$

where c_{A0} is the concentration in the A zone when it is coincident with the B zone. If t' is the time required to separate the A and B zone by a distance Δx_{AB}, a distance which can readily be determined experimentally, then $t' = \Delta x_{AB}/(v_A - v_B)$, and one obtains the following expression for the fraction of A molecules retained by B (or more precisely the fraction which has failed to escape in the forward direction)

$$f_r = \exp\left\{-\frac{v_{AB} - v_B}{v_A - v_B}\frac{\Delta x_{AB}}{w_A}\right\} \qquad \text{(A3-3)}$$

Using the value for v_{AB} given above (eq A2-2), eq A3-3 may be written

$$f_r = \exp\{-(1 - f\Delta x_{AC}/\Delta x_{AB})\Delta x_{AB}/w_A\} \qquad \text{(A3-4)}$$

[12] The program is written in a dialect of Fortran IV matched to the idiosyncrasies of the Honeywell 6000 and the graphic terminal. With modification almost any computer and terminal may be used. A source listing is available from the authors.

In the low concentration limit f is given by $f = Kc_B(1 + Kc_B)$, and using this and the fact that $\Delta x_{AC} = \Delta x_{AB} + \Delta x_{BC}$, eq A3-4 becomes

$$f_r = \exp\left\{-\frac{(1 - (\Delta x_{BC}/\Delta x_{AB})Kc_B)}{1 + Kc_B}\frac{\Delta x_{AB}}{w_A}\right\} \quad \text{(A3-5)}$$

Solving for Kc_B one obtains

$$Kc_B = \frac{\Delta x_{AB}/w_A \ln f_r + 1}{\alpha \Delta x_{AB}/w_A \ln f_r - 1} \quad \text{(A3-6)}$$

Note that this expression is valid only as long as the numerator is negative (since $\ln f_r < 0$); *i.e.*

$$\Delta x_{AB}/w_A > |\ln f_r| \quad \text{(A3-7)}$$

If $v_B = v_C$, $\Delta x_{BC} = 0$ and eq (A3-5) simplifies to

$$f_r = \exp\left[-\frac{1}{1 + Kc_B}\frac{\Delta x_{AB}}{w_A}\right] \quad \text{(A3-8)}$$

which may be written

$$Kc_B = [-1 + \Delta x_{AB}/w_A \ln f_r] \quad \text{(A3-9)}$$

whose region of validity is again given by eq A3-7.

Is the Rectangular Zone Model Useful When $v_B \neq v_C$? The rectangular zone model employed above led to an expression for f_r (A3-5) whose applicability is restricted to small values of Kc_B (see eq A3-7). The origin of this restriction is that the A zone velocity is assumed to have a sharp value inside and outside the B zone. From this it follows that *no* A molecules can escape the B zone if $v_{AB} < v_B$ (*cf.* eq A3-3). During an actual transport experiment the velocities of the A molecules have a distribution whose shape depends on the dissociation rate of C, k_r. The wider this distribution for any Kc_B value, and velocity ratios, the greater is the escape rate of A molecules and the smaller is f_r for a particular value of $\Delta x_{AB}/w_A$. Since f_r is dependent on the kinetic parameter k_r this case falls outside the scope of the present paper. It should be noted, however, that when $v_B = v_C$, v_{AB} always exceeds v_B and the rectangular zone model not only provides a reasonable basis for showing how f_r depends on the experimental parameters but, as can be seen from Figure 11, eq A3-8 is in rough agreement with the computer simulated results which are based on gaussian line shapes and the kinetic regime in which $k_r > v_{AB}/w_B$. In analyzing the results of an experiment the curves shown in Figure 11 are of course to be preferred to eq A3-8.

Appendix 4

Stoichiometry of Reactants. In order to ascertain that the reactants A and B are stoichiometrically equal in C, equivalent to eq 1, the following protocols are offered for the various experimental situations one encounters.

I. Homodromous Reactants ($v_A/v_B \approx 1$). The recommended loading ratio for determining K is the equimolar one. The applicability of eq 1 can be checked in two ways. First, the profiles $c_A(x)$ and $c_B(x)$ may be determined with loading ratios l_A/l_B of, say, 2, 1, and 0.5. The magnitude of the monomer peak at x_A ($= x_B$) will be of the order of $c_T/2$ when l_A/l_B is 2 or 0.5 and vanishes when and only when eq 1 applies. Alternatively, if it is inconvenient to monitor $c_A(x)$ and $c_B(x)$ separately, one may use the curve of Figure 5 to determine an apparent K value for three loading ratios such as the ones listed above. The apparent K will then be independent of the loading ratio if the reaction is A + B $\rightleftarrows$ C. If the reaction 2A + B $\rightleftarrows$ C the apparent K values will increase monotonically with increasing values of l_A/l_B, and if the reaction is of the type A + 2B $\rightleftarrows$ C, the apparent K values decrease monotonically with increasing loading ratios.

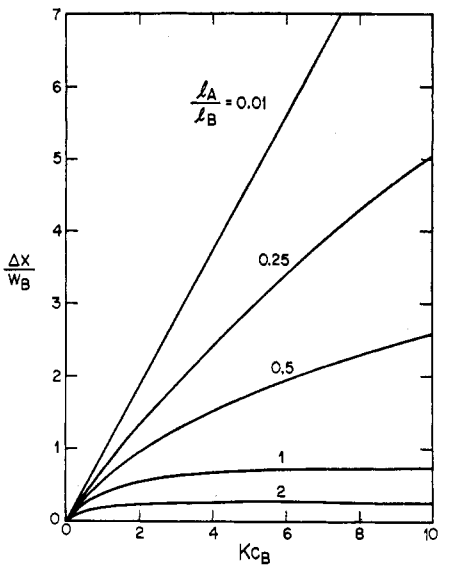

FIGURE 16: The retardation of the A zone upon passing through the B zone as a function of Kc_B and the loading ratio, in the absence of diffusion. The curves shown are equivalent to the curve marked $w_{fA}/w_{0A} = 1$ shown in Figure 9 except that that curve refers to an infinitesimal loading ratio. The dependence of the retardation on the loading ratio may be used to check that A and B are stoichiometrically equal in C (see Appendix 4).

II. Heterodromous Reactants ($v_A > v_B$). If multiple binding sites on B are suspected, retardation experiments of the kind described in section 3 are used to obtain a value of the association constant in the low concentration limit ($l_A \ll l_B$) and assuming that in the reaction nA + B $\rightleftarrows$ C, n is unity. The experiment is then repeated with finite loading ratios, *e.g.*, $l_A/l_B \approx 0.5$. (The magnitude of the loading ratio obtaining in any particular experiment is obtained by integrating the areas of the A and B zones.) The retardations observed for finite loading ratios are smaller than for infinitesimal ones since a smaller fraction of A molecules are bound as they pass through the B zones. The dependence of $\Delta x/w_B$ upon l_A/l_B and Kc_B was obtained in simulated gel runs and is shown in in Figure 16. The value of K obtained with loading ratios between 0.25 and 1 say will be consistent with those obtained using infinitestimal loading ratios if, and only if, $n = 1$. If $n \neq 1$ and the two binding sites of B are independent and have the same K, loading ratio independent K values will be obtained by use of the curves of Figure 16 if the loading ratio is redefined as l_A/nl_B. If the multiple binding sites are cooperative or have different K's, a different dependence of retardation upon Kc_B and the loading ratio obtains. Such cases will not be covered here, but all are distinguishable from the case of $n = 1$ by the experimental protocol given.

References

Bethune, J. L., and Kegeles, G. (1961a), *J. Phys. Chem. 65*, 433.

Bethune, J. L., and Kegeles, G. (1961b), *J. Phys. Chem. 65*, 1755.

Bethune, J. L., and Kegeles, G. (1961c), *J. Phys. Chem. 65*, 1761.
Blum, A. D., Uhlenbeck, O. C., and Tinoco, I., Jr. (1972), *Biochemistry 11*, 3248.
Brandt, K. G., Kimoe, A., and Hess, G. P. (1967), *J. Biol. Chem. 242*, 3973.
Cann, J. R., and Goad, W. B. (1965), *J. Biol. Chem. 240*, 1162.
Chrambach, A., and Rodbard, D. (1971), *Science 172*, 440.
DeVault, D. (1943), *J. Amer. Chem. Soc. 65*, 532.
Eisinger, J. (1970), *Biochem. Biophys. Res. Commun. 43*, 854.
Eisinger, J. (1971), *Biochem. Biophys. Res. Commun. 44*, 1135.
Fersht, A. R., and Requena, Y. (1971), *J. Mol. Biol. 60*, 279.
Gilbert, G. A., and Jenkins, R. C. (1959), *Proc. Roy. Soc., Ser. A 253*, 420.
Kegeles, G., Rhodes, L., and Bethune, J. L. (1967), *Proc. Nat. Acad. Sci. U. S. 58*, 45.
Longsworth, L. G., and McInnes, D. A. (1942), *J. Gen. Physiol. 25*, 507.
Nichol, L. W., Bethune, J. L., Kegeles, G., and Hess, E. L. (1964), *Proteins 2*, Chapter 9.
Oberhauser, D. F., Bethune, J. L., and Kegeles, G. (1965), *Biochemistry 4*, 1878.
Richards, E. G., and Lecanidou, R. (1971), *Anal. Biochem. 40*, 43.
Tiselius, A. (1930), *Nova Acta Regiae Soc. Sci. Upsal.* [4] 7, 1.
Uhlenbeck, O. C. (1972), *J. Mol. Biol. 65*, 25.
Uhlenbeck, O. C., Baller, J., and Doty, P. (1970), *Nature (London) 225*, 508.

Calorimetric Study of Protein Transitions in Human Erythrocyte Ghosts†

William M. Jackson, John Kostyla, John H. Nordin, and John F. Brandts*

ABSTRACT: Using differential heat capacity calorimetry, several well-defined thermal transitions can be detected for human erythrocyte ghosts at pH 7.4. These structural transitions are totally irreversible and are not seen for vesicles formed from lipid extracts of erythrocyte membranes and therefore must be due to thermal denaturation of membrane-bound proteins. It is shown that one bound enzyme (ATPase) does in fact lose its activity in the temperature region where the calorimetric transitions are observed. The denaturation pattern shows a strong dependence on ionic strength and this might be correlated with changes in the degree of protein–protein association on the membrane, which also shows a marked ionic strength dependence as judged by the freeze–fracture electron micrographs of Pinto da Silva (*J. Cell Biol. 53*, 777 (1972)). At an ionic strength of 0.07 M, calorimetric scans show four sharp and well-defined transitions which suggest that the bulk of the membrane protein may be organized into only a few different types of structural units.

With the fairly general acceptance of the bilayer as the basic structural framework of lipids in membranes, the major questions which are now posed concern the structure of membrane-bound protein molecules, the way in which proteins are organized in and on the membrane, and the identification of any alterations in the basic bilayer structure which might occur as a result of protein–lipid interactions. These are difficult questions to answer since solution methods applicable to membrane suspensions generally do not provide very detailed information about absolute structure and organization of protein molecules. One meaningful way of approaching the problem is to study changes in structure which occur in response to changes in solvent conditions. Hopefully, some conclusions about absolute structure can then be deduced. This approach has, in fact, been moderately productive of new information when applied to the phase transitions of lipid vesicles and of the lipid phase in membranes, but has not been widely applied to order–disorder transitions of membrane-attached proteins. Perhaps the reason for this is that the membrane proteins constitute a less cooperative system and transitions are therefore more difficult to study.

The most general technique for investigating structural transitions is calorimetry, since any process having a significant energy change may be detected. The utility of differential scanning calorimetry for detecting thermally induced phase changes in biological membranes has been demonstrated with studies of the plasma membrane of *Mycoplasma laidlawii* (Steim *et al.*, 1969; Melchoir *et al.*, 1970). For whole membranes two thermal transitions were observed; a reversible transition attributed to a phase change in the lipid bilayer and a smaller irreversible transition at higher temperature attributed to unfolding of the membrane protein.

Human erythrocyte ghosts have previously been examined by calorimetry (Chapman, 1968; J. Steim, personal communication) but no thermal transitions could be detected when using conventional DSC instruments which are adequate for studying lipid phase changes in other membranes. Using a more sensitive differential heat capacity calorimeter (Jackson and Brandts, 1970; Jackson, 1970) we have studied thermal transitions in human erythrocyte membranes as a function of solvent conditions and have examined the thermal behavior of lipid extracts from these membranes. In addition, we have investigated the thermal stability of a membrane bound enzyme function (ATPase).

† From the Departments of Chemistry and Biochemistry, University of Massachusetts, Amherst, Massachusetts 01002. *Received February 23, 1973.* This work was supported by a National Institutes of Health grant (GM-11071) and a grant from NASA (NGL-22-010-029). One of us (J. B.) received fellowship support from the Alfred P. Sloan Foundation during the course of this investigation.

* Author to whom all correspondence should be addressed at the Department of Chemistry.